# OH/OD Initiated Oxidation of Isoprene in the Presence of $O_2$ and NO

**Jiho Park,[†] Candice G. Jongsma,[†] Renyi Zhang,[‡] and Simon W. North*[,†]**

*Department of Chemistry, Texas A&M University, P.O. Box 30012, College Station, Texas 77842, and Department of Atmospheric Sciences, Texas A&M University, College Station, Texas 77843*

*Received: June 9, 2004; In Final Form: September 6, 2004*

The kinetics of the isoprene−OH/OD reaction in the presence of $O_2$ and NO have been studied using laser photolysis/laser-induced fluorescence. We report pressure and temperature-dependent rate constants for the addition of OH/OD to isoprene are in good agreement with previous studies. On the basis of simulations to OH cycling curves, we find a value of $(9.0 \pm 3.0) \times 10^{-12}$ molecule$^{-1}$ cm$^3$ s$^{-1}$ for the overall reaction rate constant of hydroxy peroxy radical with NO at 298 K. We report a rate constant for $O_2$ addition to the hydroxy alkyl radical of $(2.3 \pm 2.0) \times 10^{-12}$ molecule$^{-1}$ cm$^3$ s$^{-1}$ at 298 K. We find little generation of OH from the OD initiated oxidation of isoprene, and no significant differences in OH and OD cycling, suggesting that H-shift isomerization is the major pathway for $\delta$-hydroxy alkoxy radicals, in agreement with theoretical predictions.

## Introduction

The production of tropospheric ozone via the photochemical oxidation of biogenic hydrocarbons is a central issue in regional air quality. Isoprene (2-methyl-1,3-butadine) is the dominant nonmethane organic compound emitted by vegetation into the atmosphere, with a global emission rate of ∼450 Tg yr$^{-1}$ and its oxidation serves as a major source of ozone in North America during the summer months.[1,2] Due to strong diurnal emission, isoprene reacts predominantly with the hydroxyl radical (OH) whereas the reaction with $NO_3$ becomes more important at night.[3−5] Although there have been numerous studies on the detailed mechanism of isoprene oxidation, unresolved issues and discrepancies between reported kinetic data persist.

The reaction of isoprene and OH can result in four possible adducts and the initial branching ratios among these hydroxy alkyl radicals strongly influence the final product distribution.

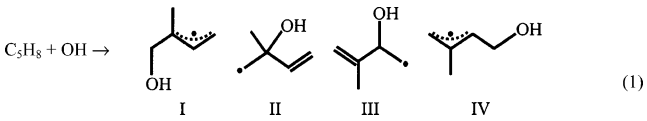

(1)

Theoretical calculations[6−9] predict that the adducts formed from OH addition to the terminal carbons (I and IV) is energetically favorable. Although estimations based on the final product analysis suggest a preference for OH addition to the terminal carbons,[10−12] a recent mass spectrometry study[8] indicates comparable yields of all four radicals. Despite the uncertainty in the initial branching ratios, there is general consensus regarding the value for the high-pressure limit reaction rate constant of $1.0 \times 10^{-10}$ molecule$^{-1}$ cm$^3$ s$^{-1}$ at 298 K with an estimated overall uncertainty of ±10%.[6,13−17] Hynes and co-workers[18] have investigated the reaction using OD as well as OH and concluded that there is a negligible isotope effect. It is worth noting that the authors have reported a rate constant of $(8.56 \pm 0.26) \times 10^{-11}$ molecule$^{-1}$ cm$^3$ s$^{-1}$, which is ∼15% lower than the recommended value. A more recent study by the same authors reported a comparable value for the rate constant, $(8.47 \pm 0.59) \times 10^{-11}$ molecule$^{-1}$ cm$^3$ s$^{-1}$.[19]

In the atmosphere the resulting hydroxy alkyl radicals react with $O_2$. Recent ab initio calculations and RRKM theory coupled with master equation calculations (RRKM/ME) by Park et al. have shown that the dominant fate of isomers II and III is prompt, i.e., nonthermal, isomerization to produce α-hydroxy isoprene radicals.[20] The authors suggest that whereas isomers I and IV react with $O_2$ via an addition mechanism to produce hydroxy peroxy radicals, the α-hydroxy isoprene radicals derived from II and III react with $O_2$ via H-atom abstraction to form C5 carbonyls. A significant yield of isomers II and III would result in a substantial yield of C5 carbonyls and a lower yield of peroxy radicals, which is inconsistent with experimental evidence.

Previous theoretical study suggests that the reaction rates associated with $O_2$ addition to the hydroxy alkyl radicals is isomer-dependent with rates varying from $1 \times 10^{-13}$ to $2 \times 10^{-12}$ molecule$^{-1}$ cm$^3$ s$^{-1}$.[21] An effective overall rate constant of $1.7 \times 10^{-12}$ molecule$^{-1}$ cm$^3$ s$^{-1}$ was found to adequately describe the R + $O_2$ reaction. Direct measurements of the rate constant for addition of $O_2$ to the hydroxy alkyl radicals are limited due to the difficulty in monitoring the hydroxy peroxy radicals. Recently Zhang et al.[22] reported the direct laboratory measurement of hydroxy peroxy radical formation using fast flow reactor coupled to chemical ionization mass spectroscopy detection and determined the rate constant of $(7 \pm 3) \times 10^{-13}$ molecule$^{-1}$ cm$^3$ s$^{-1}$. This rate constant is significantly different than an earlier report of $(2.8 \pm 0.7) \times 10^{-15}$ molecule$^{-1}$ cm$^3$ s$^{-1}$ by the same group obtained by monitoring the loss of the hydroxy alkyl radicals.[23] Interference from the decomposition of the peroxy radical cations was cited as a possible cause for the previous low value. Differences remain, however, between even the most recent value of Zhang et al. and estimated reaction rate constants from OH cycling experiments that range from $3 \times 10^{-12}$ to $8 \times 10^{-11}$ molecule$^{-1}$ cm$^3$ s$^{-1}$.[19,24−27]

In the presence of modest concentrations (>30 ppt) of $NO_x$, the hydroxy peroxy radicals react to form nitrites via NO addition. The activated nitrites promptly decompose to yield

[†] Department of Chemistry.
[‡] Department of Atmospheric Sciences.

10.1021/jp040421t CCC: $27.50 
Published on Web 11/09/2004

$\beta$- and $\delta$-hydroxy alkoxy radicals and $NO_2$.[28] Isomerization to form stable nitrates is thought to be minor (<15%) although the precise yield of this channel is the subject of some controversy.[29,30] A recent study by Sprengnether et al.[31] using infrared spectroscopy estimated a nitrate yield of 12% in agreement with the yield of 8−13% previously reported by Tuazon and Atkinson[11] on the basis of the environmental chamber experiments. In contrast, Chen et al.[32] have reported a much smaller yield of 4.4% using capillary chromatography and chemiluminescence detection. The overall rate constant for the reaction of hydroxy peroxy radicals with NO has been reported by several groups. Zhang et al.[26] reported the first direct laboratory study of the rate constant for this reaction and the predicted rate constant is $(9 \pm 3) \times 10^{-12}$ molecule$^{-1}$ cm$^3$ s$^{-1}$, consistent with the rate constants for the reaction of NO with peroxy radicals similar to isoprene based peroxy radicals.[33−35] Stevens et al.[27] reported an overall rate constant of $(1.1 \pm 0.8) \times 10^{-11}$ molecule$^{-1}$ cm$^3$ s$^{-1}$ based on cycling measurements. A similar value was recently reported by Hynes and coworkers.[19] The reported value of $(2.5 \pm 0.5) \times 10^{-11}$ molecule$^{-1}$ cm$^3$ s$^{-1}$ by Reitz et al.,[25] also based on OH cycling measurements, lies out of the error limit of those values.

The nascent alkoxy radicals formed from the decomposition of activated nitrites can decompose, isomerize, or react with $O_2$. Theoretical calculations predict that prompt decomposition is the major channel for $\beta$−hydroxy alkoxy radicals and that the fate of the $\delta$−hydroxy alkoxy radicals is prompt isomerization (*Z*-configuration).[36,37] Although there is a lack of direct experimental information regarding the fate of the alkoxy radicals, the theoretical predictions are supported by end product analysis. Simulations of the cycling data of Reitz et al.[25] suggested that the majority of hydroxy alkoxy radicals underwent thermal decomposition, in contrast to the conclusion from the theoretical study.[36] The conclusions of the early cycling experiment suffered from an overly simplified chemical mechanism that did not include important termination reactions, notably the reaction of the isoprene−OH adduct with NO. Termination at high NO concentrations was interpreted by the authors as arising from the competition between alkoxy radical decomposition and reaction with NO.[38] The final first generation end products from the decomposition of $\beta$-hydroxy alkoxy radicals are methyl vinyl ketone, methacrolein, and formaldehyde.[39−48] Prompt isomerization of $\delta$-hydroxy alkoxy radicals followed by hydrogen abstraction reaction by $O_2$ results primarily in C5 carbonyl compounds.[10,49−51]

Hydrogen abstraction by $O_2$ during the oxidation mechanism results in hydroperoxy peroxy radicals ($HO_2$) that react with NO to regenerate OH. The time-dependent kinetics of OH is thus a sensitive function of the concentration of $O_2$ and NO and can provide significant insights into the detailed mechanism of isoprene oxidation. Due to the inherent complexity of the oxidation mechanism, care must be taken to extract meaningful kinetic parameters. Sensitivity analysis provides a platform from which to assess the limitations and accuracy of kinetic simulations. Isotopic labeling experiments using OH/OD permits investigation of the competition between isomerization and hydrogen abstraction by $O_2$ for the $\delta$-hydroxy alkoxy radicals.

## Experimental Section

The detailed description of the laser photolysis/laser-induced fluorescence experiments has been reported elsewhere and only the essential features are described.[6] The unfocused 248 nm beam from the excimer laser (GAM Laser, EX10) was used to produce hydroxyl radicals from $H_2O_2$ photolysis and the beam diameter at the monitoring region was adjusted using iris to be much (~10 times) larger than the probe laser beam diameter to minimize the fly out effect. Laser-induced fluorescence was used to measure the OH/OD excited on the $Q_1(1)$ transition of the $A \leftarrow X(1,0)$ vibrational band near 282 and 287 nm for OH and OD, respectively, and each fluorescence decay was averaged for up to 100 shots. Signals were typically followed over 2 orders of magnitude decay. The measured fluence of the photolysis and probe lasers were 23.4 and 4.4 mJ/cm$^2$, respectively. The repetition rate of the lasers was set at 10 Hz and the delay between photolysis and probe lasers was controlled by a digital delay/pulse generator (SRS, DG-535). $H_2O_2$ was introduced into the cell through a flow meter by flowing argon through a bubbler containing concentrated hydrogen peroxide solution. Hydroxyl-*d* radicals were produced using the same method except using $D_2O_2$. Concentrated hydrogen peroxide was generated by vacuum distillation of 30% $H_2O_2$ (Merck) until the $H_2O_2$ concentration was determined to be 90−95% by checking the density of the solution. Typical $H_2O_2$ concentrations in the cell were $1 \times 10^{14}$ molecules cm$^{-3}$, and the hydroxyl radical concentrations were $7 \times 10^{11}$ molecules cm$^{-3}$, as estimated from the 248 nm pulse energy and the known $H_2O_2$ absorption cross section.[33] $D_2O_2$ was prepared from hydrogen/deuterium exchange by mixing excess 100% $D_2O$ (Aldrich) with concentrated $H_2O_2$ followed by vacuum distillation to obtain concentrated $D_2O_2$ solution. The reaction cell was passivated for several hours using $D_2O_2/D_2O$ prior to conducting the OD experiments. Isoprene (Aldrich, 99%) buffered with argon was prepared in a 5 L bulb via the freeze−pump−thaw method and introduced into the cell with a flow meter to yield typical isoprene concentrations of $1 \times 10^{14}$ molecules cm$^{-3}$. The NO (Aldrich, 98.5%) was buffered with argon in a 5 L bulb to known concentrations and was introduced into the cell through a flow meter. The concentrations of NO in the reaction cell were varied from 0 to $1 \times 10^{15}$ molecules cm$^{-3}$. The NO was purified to remove HONO and $NO_2$ impurities by passing it through an ascarite trap prior to mixing with argon. The rate of the reaction between $O_2$ and NO producing $NO_2$ is very slow (termolecular rate constant of $1.94 \times 10^{-38}$ cm$^6$ s$^{-1}$ molecule$^{-2}$)[52] under the present experimental conditions and was considered to be negligible in the time scale of the experiment. The typical concentration of $O_2$ in the reaction cell was $\sim 3 \times 10^{16}$ molecules cm$^{-3}$. Several experiments were run with fixed concentrations of $H_2O_2$ or $D_2O_2$, and isoprene, while the concentration of NO or $O_2$ was varied. The total pressure in the cell was varied from 2 to 8 Torr for the reaction of isoprene with hydroxyl radical in the absence of $O_2$ and NO and it was fixed at 4 Torr for the cycling experiment. The isoprene concentrations were in sufficient excess to ensure that OH reaction with the oxidation products was minor.

## Results and Discussion

**Reaction of Isoprene with OH/OD.** We have reinvestigated the initial addition reaction of isoprene with OH/OD over a temperature range of 279−336 K and a pressure range of 2−8 Torr. The pressure range was chosen to examine the falloff behavior of the reaction and to cover the range of pressures utilized in the cycling experiments. The use of $H_2O_2$ photolysis at 248 nm should provide a cleaner source of hydroxyl radicals than our previous study, which utilized the 193 nm photolysis of $HONO_2$. Figure 1 shows several bimolecular plots for the reaction of isoprene with OH taken at a total pressure of 6 Torr. Figure 2 shows the pressure dependent reaction rate constants of isoprene with OH (A) and OD (B) at various temperatures.

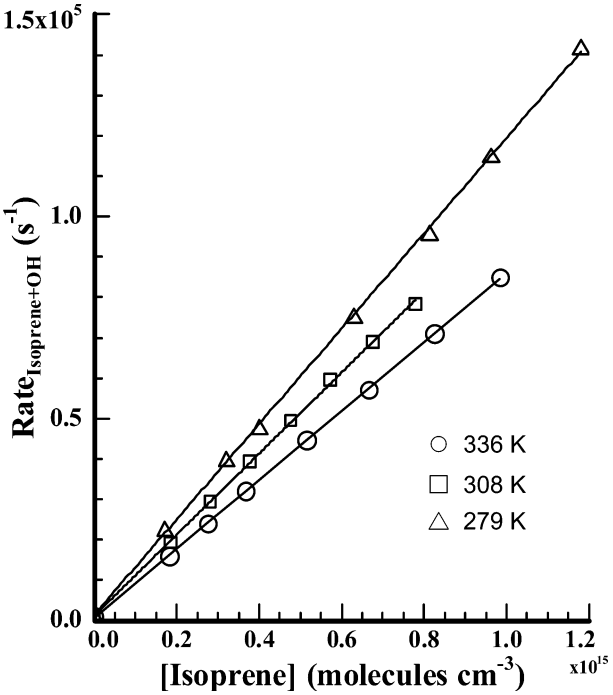


**Figure 1.** Plot of pseudo-first-order reaction rates versus isoprene concentration for the isoprene + OH reaction at 6 Torr and 279, 308, and 336 K.

Table 1 provides a summary of the measured rate constants. The pressure dependent data were fitted with the semiempirical Troe formalism,[53] widely used among atmospheric scientists to describe the falloff behavior. The expression of the form is given by

$$k([\mathrm{M}],T) = \frac{k_0(T)[\mathrm{M}]}{1 + k_0(T)[\mathrm{M}]/k_\infty(T)} F^{\{1+[\log(k_0(T)[\mathrm{M}]/k_\infty(T))]^2\}^{-1}} \quad (2)$$

where [M] is the concentration of the buffer gas, $k_0(T)$ is the low-pressure termolecular rate constant, $k_\infty(T)$ is the high-pressure limiting rate constant, and $F$ is collision broadening factor. The data were fitted using $F = 0.6$, which is recommended for atmospheric modeling[54] whereas $k_0(T)$ and $k_\infty(T)$ were determined by a nonlinear least-squares fit the data and the errors reported are at $1\sigma$. The solid lines in Figure 2 are the best fit Troe curves at each temperature. Figure 3 shows the Arrhenius plot of high-pressure rate constant for the isoprene + OH/OD reaction and the high-pressure rate constants have been obtained from extrapolation using the Troe equation. Very little difference is observed between the OH + isoprene reaction and OD + isoprene reaction, consistent with the previous study by Campuzano-Jost et al.[18] The Arrhenius plot of each reaction yields indistinguishable negative activation energies within the error limits. The derived Arrhenius rate expressions are $k_\infty(T) = (3.49 \pm 0.46) \times 10^{-11} \exp[(366 \pm 40)/T]$ molecule$^{-1}$ cm$^3$ s$^{-1}$ and $k_\infty(T) = (3.58 \pm 0.18) \times 10^{-11} \exp[(356 \pm 18)/T]$ molecule$^{-1}$ cm$^3$ s$^{-1}$ for the reaction of isoprene with OH and OD, respectively. Extrapolation of the low-pressure data to high pressures has large associated errors. However, the results predicted at 760 Torr are in reasonable agreement with the previous recommendation of $2.7 \times 10^{-11} \exp(390/T)$ molecule$^{-1}$ cm$^3$ s$^{-1}$ for the isoprene + OH reaction by Atkinson.[17] We find low-pressure termolecular rate constants of $k_0(T) = (1.16 \pm 0.88) \times 10^{-30} \exp[(3086 \pm 233)/T]$ molecule$^{-2}$ cm$^6$ s$^{-1}$ and $k_0(T) = (2.06 \pm 21.5) \times 10^{-30} \exp[(3086 \pm 3187)/T]$ molecule$^{-2}$ cm$^6$ s$^{-1}$ for OH and OD, respectively, in Ar buffer gas. Despite

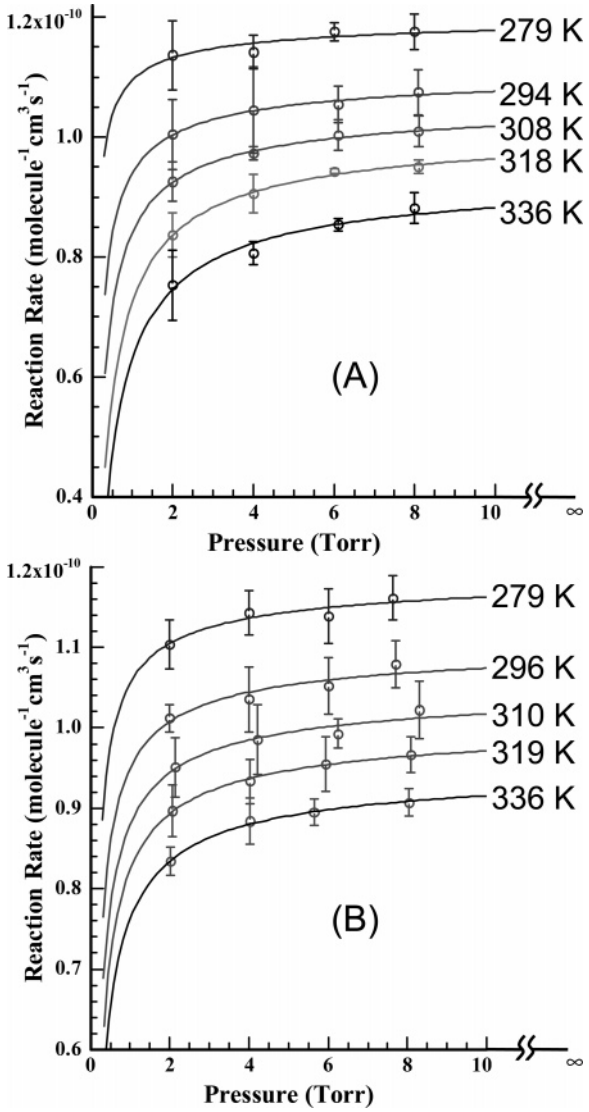


**Figure 2.** Pressure dependent rate constants for the OH/OD reaction with isoprene at several temperatures. (A) shows the reaction of isoprene with OH and (B) shows the reaction of isoprene with OD. The solid lines are fits to the data using Troe form described in the text.

the error associated with extending the low-pressure data to allow comparison with higher pressure experiments, our rate constants measured at 294 K all exceed the most recent measurements of Campuzano-Jost et al.[19] It should be noted that any systematic error in the isoprene concentration directly translates to error in the reported rate constant. The experiments of Campuzano-Jost et al.[19] involved the in situ monitoring of isoprene using UV absorption at 228 nm. The authors reported no loss of isoprene to polymerization or dark reactions, processes that, if important, would suggest that the rate constants reported in the present study are *underestimated*.

Recently, Chuong et al.[15] have investigated the falloff behavior of the OH reaction with isoprene as a function of temperature using He as a buffer. The authors determined a low-pressure termolecular rate constant expression of $k_0(T) = (9.3 \pm 0.46) \times 10^{-29} \exp[(1560 \pm 230)/T]$ molecule$^{-2}$ cm$^6$ s$^{-1}$ using the Troe form and fixing the high-pressure limit to the expression given by Atkinson. The difference between the $k_0$ reported by Chuong et al. and $k_0$ derived in this study is consistent with the previous studies comparing the use of He and Ar buffer gases.[55] Chuong et al. state that no pressure dependence was observed at room temperature down to 1 Torr.

**TABLE 1: Rate Constants for OH/OD + Isoprene Reaction**

| temp (K) | pressure (Torr) | $k$ ($cm^3$ $s^{-1}$ $molecule^{-1}$) |
|---|---|---|
| | OH + Isoprene | |
| 279 | 2.0 | $(11.4 \pm 0.29) \times 10^{-11}$ |
| | 4.0 | $(11.4 \pm 0.14) \times 10^{-11}$ |
| | 6.0 | $(11.8 \pm 0.09) \times 10^{-11}$ |
| | 8.0 | $(11.9 \pm 0.16) \times 10^{-11}$ |
| 294 | 2.0 | $(10.1 \pm 0.29) \times 10^{-11}$ |
| | 4.0 | $(10.4 \pm 0.36) \times 10^{-11}$ |
| | 6.1 | $(10.6 \pm 0.15) \times 10^{-11}$ |
| | 8.1 | $(10.8 \pm 0.19) \times 10^{-11}$ |
| 308 | 2.0 | $(9.22 \pm 0.15) \times 10^{-11}$ |
| | 4.0 | $(9.73 \pm 0.05) \times 10^{-11}$ |
| | 6.0 | $(10.0 \pm 0.13) \times 10^{-11}$ |
| | 8.1 | $(10.1 \pm 0.13) \times 10^{-11}$ |
| 318 | 2.0 | $(8.37 \pm 0.19) \times 10^{-11}$ |
| | 4.0 | $(9.06 \pm 0.16) \times 10^{-11}$ |
| | 6.0 | $(9.43 \pm 0.02) \times 10^{-11}$ |
| | 8.1 | $(9.51 \pm 0.06) \times 10^{-11}$ |
| 336 | 2.0 | $(7.53 \pm 0.29) \times 10^{-11}$ |
| | 4.0 | $(8.10 \pm 0.10) \times 10^{-11}$ |
| | 6.1 | $(8.54 \pm 0.06) \times 10^{-11}$ |
| | 8.0 | $(8.83 \pm 0.13) \times 10^{-11}$ |
| | OD + Isoprene | |
| 279 | 2.0 | $(11.0 \pm 0.15) \times 10^{-11}$ |
| | 4.0 | $(11.4 \pm 0.14) \times 10^{-11}$ |
| | 6.0 | $(11.4 \pm 0.17) \times 10^{-11}$ |
| | 7.6 | $(11.6 \pm 0.14) \times 10^{-11}$ |
| 296 | 2.0 | $(10.4 \pm 0.12) \times 10^{-11}$ |
| | 4.0 | $(10.7 \pm 0.07) \times 10^{-11}$ |
| | 6.0 | $(10.7 \pm 0.09) \times 10^{-11}$ |
| | 8.0 | $(10.8 \pm 0.13) \times 10^{-11}$ |
| 310 | 2.0 | $(9.51 \pm 0.19) \times 10^{-11}$ |
| | 4.0 | $(9.85 \pm 0.22) \times 10^{-11}$ |
| | 6.0 | $(9.95 \pm 0.09) \times 10^{-11}$ |
| | 7.9 | $(10.2 \pm 0.18) \times 10^{-11}$ |
| 319 | 2.1 | $(8.95 \pm 0.16) \times 10^{-11}$ |
| | 4.0 | $(9.34 \pm 0.14) \times 10^{-11}$ |
| | 5.9 | $(9.54 \pm 0.17) \times 10^{-11}$ |
| | 8.1 | $(9.65 \pm 0.11) \times 10^{-11}$ |
| 336 | 2.0 | $(8.33 \pm 0.09) \times 10^{-11}$ |
| | 4.0 | $(8.84 \pm 0.14) \times 10^{-11}$ |
| | 5.6 | $(8.97 \pm 0.08) \times 10^{-11}$ |
| | 8.1 | $(9.10 \pm 0.09) \times 10^{-11}$ |

However, on the basis of their reported values of $k_0(T)$ and $k_\infty(T)$ a pressure dependence similar to the dependence in Figure 2 should have been observed in contrast to the reported experimental values.

We find that the cycling experiments are insensitive to the isoprene concentration provided that the initial OH loss rate (the product of $k_1$ and the isoprene concentration) is correct.

**Reaction of Isoprene with OH/OD in the Presence of $O_2$ and NO.** In the polluted atmosphere, isoprene oxidation by OH proceeds in the presence of moderate concentrations of NO and large $O_2$ concentrations. The origin of OH regeneration in the presence $O_2$ and NO is shown schematically in Figure 4. The first intermediate radical product, $C_5H_8OH$, reacts with $O_2$ to produce the peroxy radical ($HOC_5H_8O_2$). The reaction between peroxy radicals and NO yields alkoxy radicals and nitrogen dioxide. The decomposition of alkoxy radicals, followed by the $HO_2$ + NO reaction regenerates OH radical.

Figure 5 shows a typical set of OH cycling data using concentrations of isoprene and $O_2$ of $7.5 \times 10^{13}$ and $3.43 \times 10^{16}$ molecules $cm^{-3}$, respectively. The individual curves represent various concentrations of NO ranging from 0 to $1.04 \times 10^{15}$ molecules $cm^{-3}$. Table 2 summarizes the concentrations employed in the cycling experiments. In the absence of NO, the observed OH decay shows pseudo-first-order kinetics with

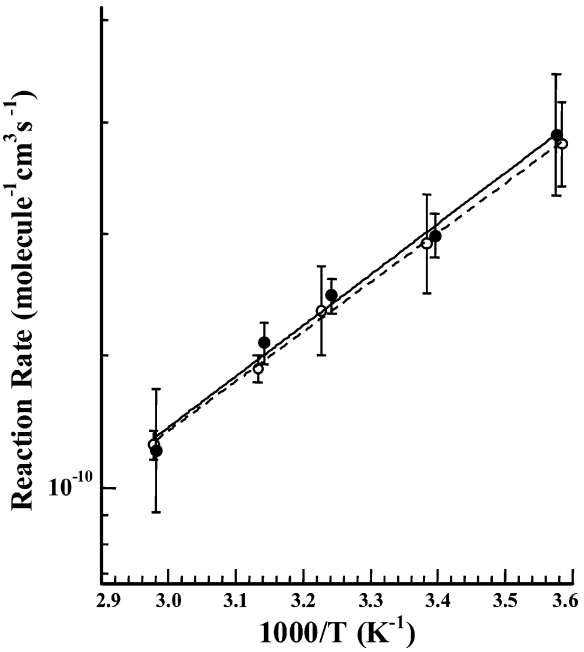


**Figure 3.** Arrhenius plots of the high-pressure rate constants, $k_\infty(T)$, for the OH (●) and OD (○) reaction with isoprene. The solid and dashed lines are the best fits to the data.

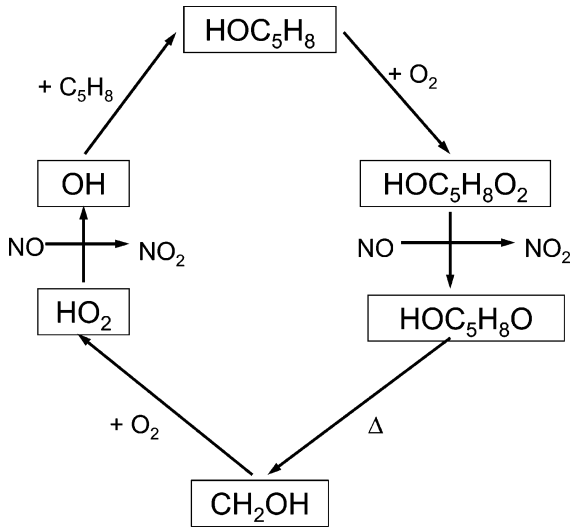


**Figure 4.** Schematic diagram illustrating the origin of OH cycling in the oxidation of isoprene.

a rate constant of $1.0 \times 10^{-10}$ $molecule^{-1}$ $cm^3$ $s^{-1}$, consistent with the recommended value. The experimental OH cycling curves exhibit several common features. At early times the curves decrease exponentially with a time constant consistent with reaction 1 (Table 3) until the onset of cycling near 300−400 $\mu$s, finally reaching steady state at long times. As the concentration of NO is increased, the onset of cycling occurs at earlier reaction times and the curves then show a slow decay due to termination reactions that act as OH sinks.

A numerical program, KINTECUS,[56] was used to simulate the data from the experiments and the sensitivity analysis was performed using the same software. The 14 reactions used in the simulations are given in Table 3 along with the rate constants corresponding to each step. The best fits of the simulations to the data are shown as solid lines in Figure 5. The reaction scheme includes reactions for which the simulations were sensitive (vide infra) and were required for adequate fitting. A more detailed 44 reaction mechanism that includes self-reactions

**TABLE 2: Experimental Conditions for OH/OD Cycling Studies at 298 K and 4 Torr**

| P | $[C_5H_8]$ ($10^{14}$ molecules $cm^{-3}$) | $[O_2]$ ($10^{16}$ molecules $cm^{-3}$) | [NO] ($10^{14}$ molecules $cm^{-3}$) |
|---|---|---|---|
| | | OH + Isoprene | |
| 2 | 1.7−10.2 | | |
| 4 | 1.8−9.9 | | |
| 6 | 1.6−11.8 | | |
| 8 | 1.7−12.0 | | |
| | | OD + Isoprene | |
| 2 | 1.8−11.1 | | |
| 4 | 1.3−9.0 | | |
| 6 | 1.5−10.8 | | |
| 8 | 1.3−10.7 | | |
| | | OH + Isoprene + $O_2$ + NO | |
| 4 | 0.75 | 3.45 | 2.65 |
| | | | 3.38 |
| | | | 4.42 |
| | | | 5.26 |
| | | | 7.24 |
| | | | 8.90 |
| | | | 10.4 |
| | 0.87 | 0.51 | 10.6 |
| | | 0.81 | |
| | | 1.39 | |
| | | 3.47 | |
| | | OD + Isoprene + $O_2$ + NO | |
| | 0.75 | 3.45 | 2.65 |
| | | | 4.42 |
| | | | 7.24 |
| | | | 10.4 |

[OH] or [OD]: $<1 \times 10^{12}$ molecules $cm^{-3}$

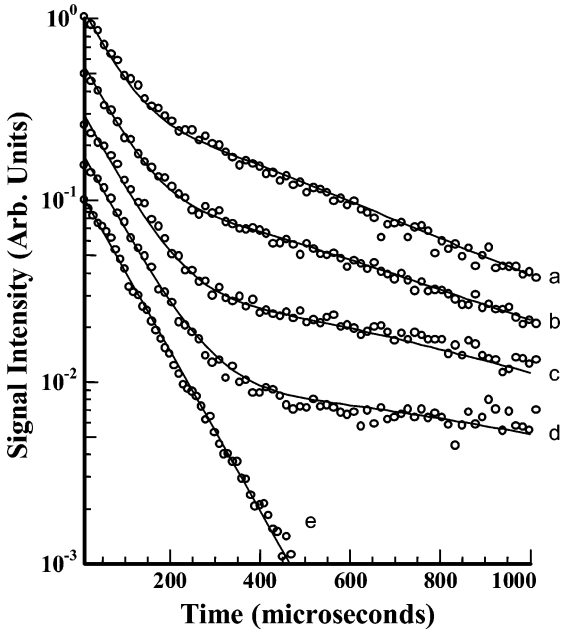


**Figure 5.** OH decays at several NO concentrations. Circles represent experimental data, and lines represent the fits using the reaction mechanism and rate constants in Table 3 with $[C_5H_8] = 7.5 \times 10^{13}$ molecules $cm^{-3}$ and $[O_2] = 3.45 \times 10^{16}$ molecules $cm^{-3}$. The plots labeled a−d correspond to NO concentrations of $10.4 \times 10^{14}$, $7.24 \times 10^{14}$, $4.42 \times 10^{14}$, and $2.65 \times 10^{14}$ molecules $cm^{-3}$, respectively. The last plot, labeled e, was taken in the absence of NO.

of the radical species present in this system and other side reactions was also used to simulate the data (Table S1). The OH-simulation curves using either the 14 or 44 reaction schemes were indistinguishable.[57] This is not to suggest that such a simplified mechanism can be applied to atmospheric models and is only a consequence of the low $O_2$ concentrations and high NO concentrations employed in present study which makes the kinetics insensitive to many of the side reactions involving $O_2$. Many of these reactions, in particular the alkoxy radical reactions with $O_2$, will be important under ambient conditions. The mechanism in Table 3 cannot predict the yields of first generation end products because these are sensitive to the initial branching of OH addition to the two terminal carbons of isoprene (eq 1) which is not specified (the products of reactions $k_7$, $k_8$, and $k_{10}$ are not specified). However, adjusting the relative yields of isomers I and IV to be 0.62:0.31, the detailed reaction mechanism in Table S1 predicts the product distribution given in Table 4.[58] This branching ratio between isomers I and IV is close to previous theoretical prediction[7] and structure activity relationship studies by Peeters et al.[59] Table 4 also shows a comparison between the end-product distribution and the experimental product yields reported by other groups. The end-product yields are relatively insensitive to the both the NO concentration and the nitrate yield.

The rate constant 1 has been well established,[6,13−17] and we have adopted a value of $1.0 \times 10^{-11}$ $cm^3$ $molecule^{-1}$ $s^{-1}$ in our mechanism on the basis of the pressure and temperature-dependent data shown in Figure 2. The initial branching ratio of OH addition to the internal carbons of isoprene was chosen to be 0.07 on the basis of the previous calculations,[6] and we have used an effective rate constant of $7 \times 10^{-12}$ $cm^3$ $molecule^{-1}$ $s^{-1}$ for this reaction in the 44 reaction simulation. When this rate constant is small there is no difference between the detailed mechanism that includes this reaction and the reduced mechanism that ignores internal addition. When the rate constants for the OH addition reaction to the internal and terminal carbons of isoprene are comparable, the mechanisms

**TABLE 3: Reduced Reaction Mechanism and Corresponding Rate Constants (298 K) Used To Simulate the OH Cycling Experiments**

| reaction | rate constant |
|---|---|
| 1. $OH + C_5H_8 \rightarrow HOC_5H_8$ | $1.0 \times 10^{-10}$ $cm^3$ $molecule^{-1}$ $s^{-1}$ |
| 2. $HOC_5H_8 + O_2 \rightarrow HOC_5H_8O_2$ | $2.3 \times 10^{-12}$ $cm^3$ $molecule^{-1}$ $s^{-1}$ |
| 3. $HOC_5H_8 + NO \rightarrow HOC_5H_8NO$ | $1.5 \times 10^{-11}$ $cm^3$ $molecule^{-1}$ $s^{-1}$ |
| 4. $HOC_5H_8O_2 + NO \rightarrow HOC_5H_8ONO_2$ | $4.5 \times 10^{-13}$ $cm^3$ $molecule^{-1}$ $s^{-1}$ |
| 5. $HOC_5H_8O_2 + NO \rightarrow HOC_5H_8O + NO_2$ | $8.55 \times 10^{-12}$ $cm^3$ $molecule^{-1}$ $s^{-1}$ |
| 6. $HOC_5H_8O \rightarrow HOC_5H_7OH$ | prompt (32%) |
| 7. $HOC_5H_8O \rightarrow CH_2OH$ + products | prompt (63%) |
| 8. $HOC_5H_8O \rightarrow CH_2OH$ + products | $5 \times 10^5$ $s^{-1}$ (5%) |
| 9. $HOC_5H_8O + NO \rightarrow HOC_5H_8ONO$ | $3 \times 10^{-11}$ $cm^3$ $molecule^{-1}$ $s^{-1}$ |
| 10. $HOC_5H_7OH + O_2 \rightarrow HO_2$ + products | $1 \times 10^{-11}$ $cm^3$ $molecule^{-1}$ $s^{-1}$ |
| 11. $HOC_5H_7OH + NO \rightarrow HOC_5H_8OHNO$ | $3 \times 10^{-11}$ $cm^3$ $molecule^{-1}$ $s^{-1}$ |
| 12. $CH_2OH + O_2 \rightarrow HO_2 + HCHO$ | $9.1 \times 10^{-12}$ $cm^3$ $molecule^{-1}$ $s^{-1}$ |
| 13. $CH_2OH + NO \rightarrow CH_2OHNO$ | $1.15 \times 10^{-11}$ $cm^3$ $molecule^{-1}$ $s^{-1}$ |
| 14. $HO_2 + NO \rightarrow OH + NO_2$ | $8.85 \times 10^{-12}$ $cm^3$ $molecule^{-1}$ $s^{-1}$ |

**TABLE 4: First Generation End Products Predicted from the Oxidation Mechanism under Ambient Conditions ($[O_2] = 4.8 \times 10^{18}$, $[NO] = 2.5 \times 10^{14}$)**

| product[a] | this work | ref 42 | ref 70 | ref 71 | ref 45 |
|---|---|---|---|---|---|
| MVR | 35.7 | $29 \pm 7$ | 33.1 | | $32 \pm 5$ |
| MACR | 25.5 | $21 \pm 5$ | 22.2 | | $22 \pm 2$ |
| formaldehyde | 63.7 | ca. 50 | 65.6 | | $57 \pm 6$ |
| $C_4$-carbonyl | 2.5 | | | 3.3 | |
| $C_5$-carbonyl | 31.0 | ca. 25 | 20.2 | 27.7 | |

[a] MVK, methlyvinyl ketone; MACR, methacrolein.

yield different results and simulations using the detailed mechanism were not satisfactory. The origin of the difference in the cycling curves arises because internal addition leads to *prompt* $HO_2$ production via ring cyclization to produce α-hydroxy radicals[20] whereas $HO_2$ production from initial terminal addition requires several intermediate steps.

The rate constant for the reaction between $CH_2OH$ and $O_2$ as well as the rate constant for the reaction between NO and $HO_2$ are also well-known and we have used room-temperature rate constants of $9.1 \times 10^{-12}$ and $8.85 \times 10^{-12}$ cm$^3$ molecule$^{-1}$ s$^{-1}$, respectively.[17,33]

At high NO concentrations the mechanism *must* include termination steps arising from the addition NO to radical species. The rate constant for the alkoxy reaction, $k_9 = 3 \times 10^{-11}$ cm$^3$ molecule$^{-1}$ s$^{-1}$, is based on the recommendation by Atkinson[60] for similar reactions and the work by Lotz and Zellner who determined a rate constant of $(3.9 \pm 0.3) \times 10^{-11}$ cm$^3$ molecule$^{-1}$ s$^{-1}$ for the reaction of the 2-butoxyl radical with NO.[61] The authors also found that the reaction was independent of total pressure from 5 to 80 Torr. Work by Dibble and co-workers[62] and Seakins and co-workers[63] also support adopting a pressure independent rate constant of $3 \times 10^{-11}$ cm$^3$ molecule$^{-1}$ s$^{-1}$ for this reaction. We have used a rate constant of $1.5 \times 10^{-11}$ cm$^3$ molecule$^{-1}$ s$^{-1}$ for the reaction of the isoprene−OH radicals with NO which is slightly larger than the value for the $CH_2OH$ + NO reaction. Sensitivity analysis demonstrates that the OH cycling curves are most sensitive to these termination rates at the highest NO concentrations employed in this study.

The reactions in the oxidation mechanism that arise from activated, nonthermal, species have rates that exceed or are comparable to the collision frequency and are therefore treated as instantaneous on the time scale of the overall kinetics. We have denoted these reactions as *prompt* in Table 3 and the simulations are insensitive to the value utilized provided the rate constants were $>1 \times 10^6$ s$^{-1}$. The percentages provided in Table 3 refer to branching ratios based on previous theoretical predictions; reaction 6 corresponds to the fraction of δ-hydroxy alkoxy radicals that undergo prompt isomerization according to refs 37, reaction 7 corresponds to the fraction of β-hydroxy alkoxy radicals which undergo prompt decomposition according to ref 36, and reaction 8 corresponds to thermalized β-hydroxy alkoxy radicals which undergo decomposition. The reader is referred to the Supporting Information, where the β- and δ-hydroxy alkoxy radicals are treated explicitly, for further clarification.

**$RO_2$ + NO Reaction Rate Constant.** The current experimental study seeks to deduce the rate constants for the intermediate reactions from the measurement of the time-dependent hydroxyl radical concentration. It is necessary, therefore, to investigate whether the combination of experimental conditions given the chemical mechanism can provide reliable kinetic parameters. Sensitivity analysis can afford an assessment of the dependence of the data to specific rate constants in the reaction mechanism.[64] The normalized sensitivity coefficients (NSC) describes the dependence of the concentration of OH on each rate constant in the chemical mechanism,

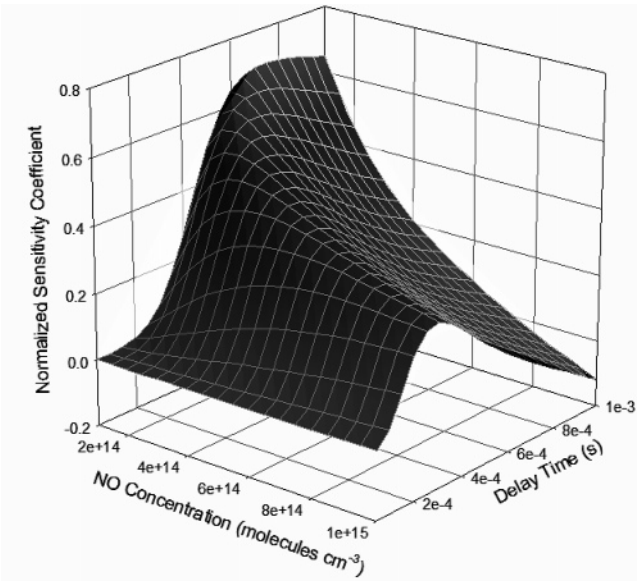


**Figure 6.** 3D plot of normalized sensitivity coefficient (NSC) of the reaction of hydroxy peroxy radical with NO ($k_4 + k_5$ in Table 3) assuming $[C_5H_8] = 7.5 \times 10^{13}$ molecules cm$^{-3}$ and $[O_2] = 3.45 \times 10^{16}$ molecules cm$^{-3}$.

$$\mathrm{NSC}_i = \left( \frac{\frac{\partial [\mathrm{OH}]}{[\mathrm{OH}]}}{\frac{\partial k_i}{k_i}} \right)_i = \left( \frac{\partial \ln [\mathrm{OH}]}{\partial \ln k_i} \right)_i \qquad (3)$$

where $k_i$ represents the rate constant of the $i^{\text{th}}$ step in the reaction mechanism and [OH] represents the concentration of the hydroxyl radical at the specific time. An NSC of 1.0, for example, indicates that a 10% change in the rate constant *i* results in a 10% change in the OH concentration at a given time. Figure 6 shows NSC for the rate constant of hydroxy peroxy radical with NO ($k_5$) as a function of NO concentration and reaction time based on the reaction mechanism in Table 3. The sensitivity of the data to the rate constant increasing as the concentration of NO decreases and is at a maximum value near the onset of cycling (~400 μs). Figure 7 shows NSCs for all the rate constants in the reaction mechanism evaluated at a low NO concentration ($2.65 \times 10^{14}$ molecules cm$^{-3}$) and 400 μs reaction time. The figure demonstrates that the OH concentration profile depends sensitively on relatively few rate constants, in particular $k_1$ and $k_5$, and is insensitive to others. Although the NSC for the NO + $HO_2$ rate constant is comparable with that for the peroxy radical reaction with NO, the NO + $HO_2$ reaction is well studied and the reported rate constant has associated uncertainty. We find that a value of $(k_4 + k_5) = (9.0 \pm 3.0) \times 10^{-12}$ molecule$^{-1}$ cm$^3$ s$^{-1}$ for the overall reaction rate constant of hydroxy peroxy radical with NO provides the best fit to the experimental data (Figure 8). The dotted lines represent error limits, and the solid line is the best fit. The value is consistent with the rate constant previously reported.[25,26,33−35] We find that the present experiments are not sensitive to the nitrate yield given the experimental conditions and we have adopted a value of 5% that is close to the value proposed by Chen et al.[32] The rate constant for the reaction of hydroxy peroxy radical with NO is substantially higher that the value of $3.8 \times 10^{-12}$

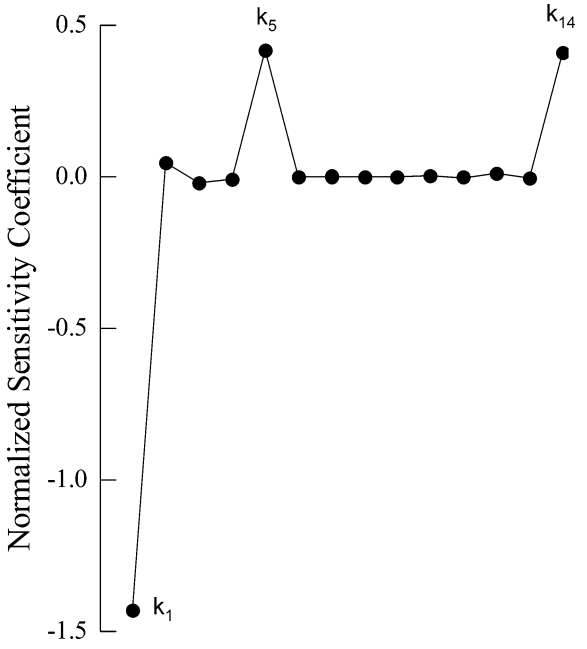


**Figure 7.** Normalized sensitivity coefficients at the delay time of 400 $\mu$s with $[C_5H_8] = 7.5 \times 10^{13}$ molecules cm$^{-3}$, $[O_2] = 3.45 \times 10^{16}$ molecules cm$^{-3}$, and $[NO] = 2.65 \times 10^{14}$ molecules cm$^{-3}$, respectively.

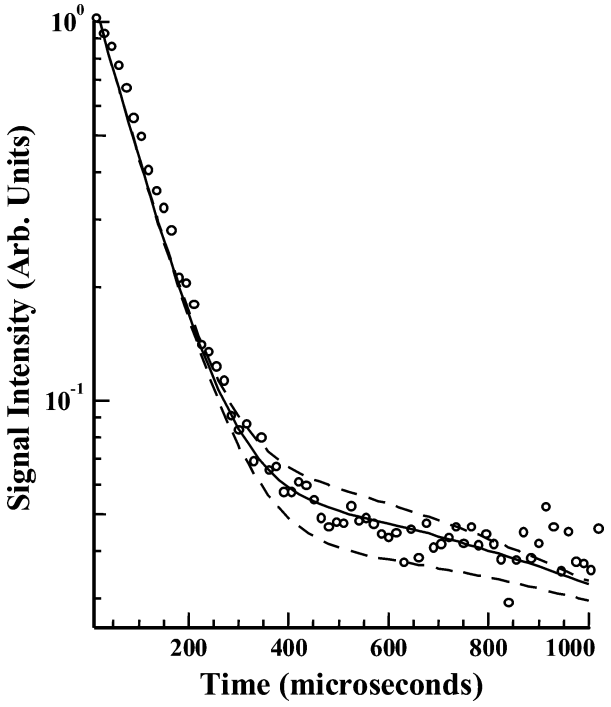


**Figure 8.** OH decay with $[NO] = 2.65 \times 10^{14}$ molecules cm$^{-3}$. Circles represent data, and the solid line is a simulation using parameters in Table 3. The dashed lines show the estimated error ranges for the rate constant of the reaction between hydroxy peroxy radical and NO ($k_4 + k_5$). $[C_5H_8] = 7.5 \times 10^{13}$ molecules cm$^{-3}$ and $[O_2] = 3.45 \times 10^{16}$ molecules cm$^{-3}$.

molecule$^{-1}$ cm$^3$ s$^{-1}$ proposed by Jenkin and Hayman[12] using the expression $(k_4 + k_5) = 7.6 \times 10^{-12} \exp[-0.17(n - 1)]$ molecule$^{-1}$ cm$^3$ s$^{-1}$, where $n$ is the number of carbons. The expression is based on studies by Wallington and co-workers[65] who reported a decrease in rate constant with the size of organic group. The reported value of $(k_4 + k_5) = (2.5 \pm 0.5) \times 10^{-11}$ molecule$^{-1}$ cm$^3$ s$^{-1}$ by Reitz et al.[25] is higher than the present value, and outside the mutual error limits. We believe that a potential source of the error in ref 25 was the high isoprene concentrations (>$1 \times 10^{14}$ molecules cm$^{-3}$) and photolysis power employed, which resulted in the production of hydrogen atoms from isoprene photodissociation. These hydrogen atoms react with $O_2$ to provide a prompt source of $HO_2$ and, therefore, OH regeneration.

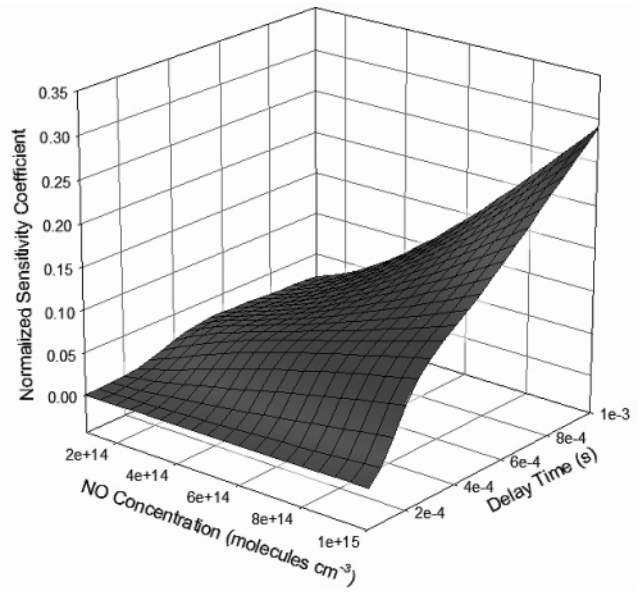


**Figure 9.** 3D plot of normalized sensitivity coefficient (NSC) of the reaction of hydroxy alkyl radical with $O_2$ ($k_2$ in Table 3) assuming $[C_5H_8] = 7.5 \times 10^{13}$ molecules cm$^{-3}$ and $[O_2] = 3.45 \times 10^{16}$ molecules cm$^{-3}$.

**R + $O_2$ Reaction Rate Constant.** At moderate to high concentrations of NO sensitivity analysis predicts a reasonable NSC for the rate constant of $O_2$ addition to the hydroxy alkyl radical. Figure 9 shows the dependence of the NSC for $k_2$ as a function of time delay and NO concentration. Assuming the rate constant of $9.0 \times 10^{-12}$ molecule$^{-1}$ cm$^3$ s$^{-1}$ for the hydroxy peroxy radical reaction with NO, the rate constant was determined to be $(2.3 \pm 2.0) \times 10^{-12}$ molecule$^{-1}$ cm$^3$ s$^{-1}$. The pressure dependence of this particular reaction has not been measured to our knowledge. However, a comparison with other analogous reactions of $O_2$ with hydroxyalkyl radicals suggests that even at the pressures of our experiments the reaction can be considered in the high-pressure limit.[66] Although the exact value of the rate constant is unimportant under atmospheric conditions, the value is necessary for accurate modeling of laboratory kinetics studies. The simulation of the reaction with the NO concentration of $1 \times 10^{15}$ molecules cm$^{-3}$ is shown in Figure 10. The rate constant we have determined is similar to the value of $1.75 \times 10^{-12}$ molecule$^{-1}$ cm$^3$ s$^{-1}$ calculated recently by Lei et al.[21] Koch et al. reported that the hydroxyalkyl radicals, formed from the reaction of OH with isoprene, reacted with $O_2$ at a rate of approximately $0.6 \times 10^{-12}$ cm$^3$ molecule$^{-1}$ s$^{-1}$ and $2.0 \times 10^{-12}$ cm$^3$ molecule$^{-1}$ s$^{-1}$ at 345 and 300 K, respectively, based on cycling experiments.[67] The rate also agrees with the rates on the order of $10^{-12}$ molecule$^{-1}$ cm$^3$ s$^{-1}$ reported by Atkinson[60] for alkyl radicals. Our rate constant, however, is lower than reported in recent cycling experiments. Stevens et al. have used a value of $6.9 \times 10^{-12}$ cm$^3$ molecule$^{-1}$ s$^{-1}$ (ref 24), subsequently $2.8 \times 10^{-11}$ cm$^3$ molecule$^{-1}$ s$^{-1}$ (ref 27), and Campuzano-Jost et al.[19] reported a value of $8 \times 10^{-12}$ molecule$^{-1}$ cm$^3$ s$^{-1}$ for this reaction at 298 K. We are unable to achieve satisfactory fits to the data using values that are larger than $5 \times 10^{-12}$ cm$^3$ molecule$^{-1}$ s$^{-1}$ at low $O_2$ concentrations where the OH cycling curves are most sensitive to this reaction. In the experiments of Campuzano-Jost et al. the termination

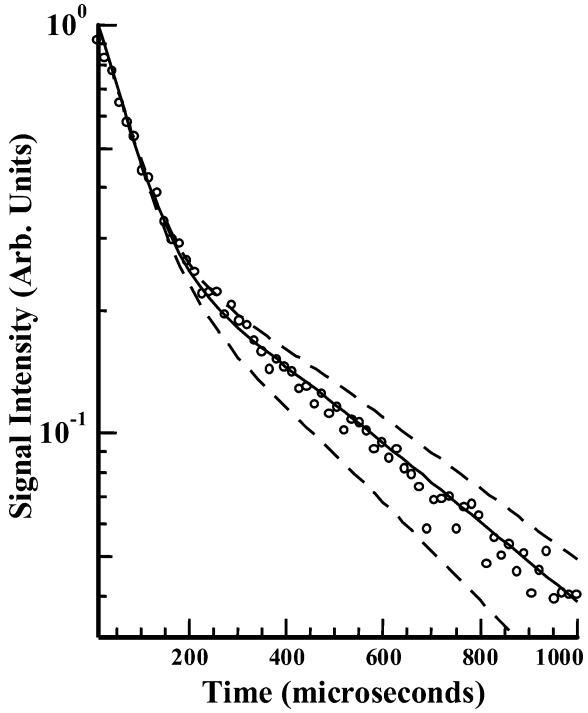


**Figure 10.** OH decay at [NO] = $1.04 \times 10^{15}$ molecules cm$^{-3}$. Circles represent data, and the solid line is a simulation using parameters in Table 3. The dashed lines show the estimated error ranges for the rate constant of the reaction between hydroxy alkyl radical and $O_2$ ($k_2$). [$C_5H_8$] = $7.5 \times 10^{13}$ molecules cm$^{-3}$ and [$O_2$] = $3.45 \times 10^{16}$ molecules cm$^{-3}$.

reaction of the isoprene−OH radicals with NO was not included in the reaction and becomes competitive with the $O_2$ reaction at lower $O_2$ concentrations. This reaction is omitted from the MCM because it is unimportant under ambient conditions. A dramatic example is illustrated in Figure 11, which shows a set of cycling curves taken with lower $O_2$ concentrations where the rates of $O_2$ addition and NO termination are comparable. Simulations based on the mechanism in Table 3 are shown in the top panel, and simulations based on the mechanism proposed in ref 19 are shown in the lower panel. Under these conditions the MCM mechanism underestimates the role of termination although this affect is less pronounced at higher $O_2$ concentrations.[68] In the experiments of Stevens and co-workers much higher $O_2$ concentrations ($\sim 1 \times 10^{16}$) than NO concentrations ($\sim 1 \times 10^{13}$) were used, which decreased the sensitivity to the R + $O_2$ rate and the value of $k_2[O_2]$ was greater than $1 \times 10^3$ s$^{-1}$, which was prompt in their experimental time scale. The error provided in the paper was a limit determined by adjusting $k_2$ until the simulation gives an unacceptable fit to the data.

**Isotopically Labeled Cycling Experiments.** The 248 nm photolysis of $D_2O_2$ generates OD in the presence of isoprene, $O_2$, and NO. The time-dependent concentration of OD or OH is monitored independently using LIF. Figure 12 shows the OD cycling at different NO concentrations using identical concentrations as in the OH experiments to facilitate comparison. The set of curves using the extended mechanism, which differentiates between the alkoxy channels, is nearly indistinguishable from the OH cycling curves (Figure 5). The simulations to the curves used rate constants identical to those given in Table 3. Based on the negligible difference between OH and OD initiated oxidation, it is possible to assess the branching ratio between hydrogen abstraction by $O_2$ and isomerization followed by hydrogen abstraction by $O_2$ for the $\delta$-hydroxy alkoxy radical.

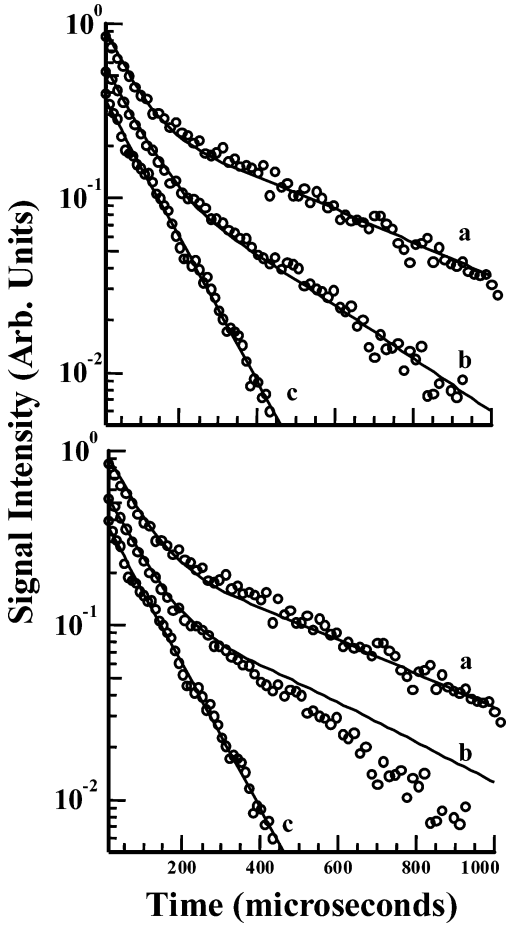


**Figure 11.** OH decays at several $O_2$ concentrations. Circles represent experimental data, and lines represent kinetic simulations. [$C_5H_8$] = $7.1 \times 10^{13}$ molecules cm$^{-3}$ and [NO] = $1.03 \times 10^{15}$ molecules cm$^{-3}$. The plots labeled a and b correspond to $O_2$ concentrations of $3.5 \times 10^{16}$ molecules cm$^{-3}$ and $6.9 \times 10^{14}$ molecules cm$^{-3}$, respectively. The last plot, labeled c, was taken in the absence of NO. Simulations based on the mechanism in Table 3 are shown in the top panel and simulations based on the mechanism proposed in ref 19 are shown in the lower panel.

These reaction channels are shown below for a particular $\delta$-hydroxy alkoxy radical.

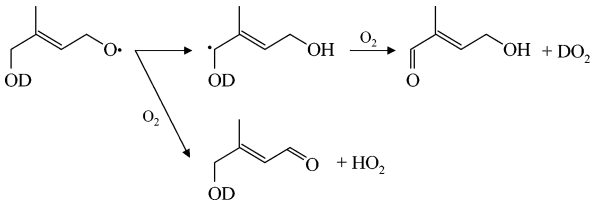


(4)

In the case of OD initiated oxidation, isomerization, followed by H-atom abstraction, would lead to the regeneration of OD whereas direct H-atom abstraction would lead to the loss of OD and production of OH. A comparison of Figures 5 and 12 suggests that isomerization (top scheme) is the preferred pathway for the $\delta$-hydroxy alkoxy radicals, consistent with recent theoretical work by Dibble[37] and Zhao et al.[69]

A more compelling illustration of fate of the $\delta$-hydroxy alkoxy radicals can be seen in Figure 13, which shows both the OD and OH concentrations for the OD initiated oxidation of isoprene in the presence of $O_2$ and NO. The intensity of the OH and OD signals is shown on a relative scale and the initial concentration of OD from $D_2O_2$ is about 2 orders of magnitude larger than that of OH. Every effort was made to ensure identical

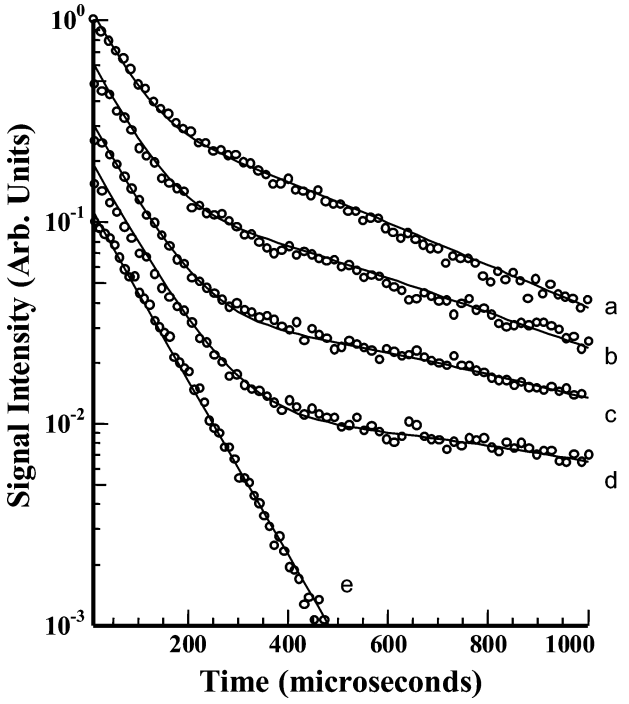


**Figure 12.** OD decays at several NO concentrations. Circles represent experimental data, and lines represent the fits using the reaction mechanism and rate constants in Table 3 with $[C_5H_8] = 7.5 \times 10^{13}$ molecules $cm^{-3}$ and $[O_2] = 3.45 \times 10^{16}$ molecules $cm^{-3}$. The plots labeled a, b, c, and d correspond to NO concentrations of $10.4 \times 10^{14}$, $7.24 \times 10^{14}$, $4.42 \times 10^{14}$, and $2.65 \times 10^{14}$ molecules $cm^{-3}$, respectively. The last plot, labeled e, was taken in the absence of NO.

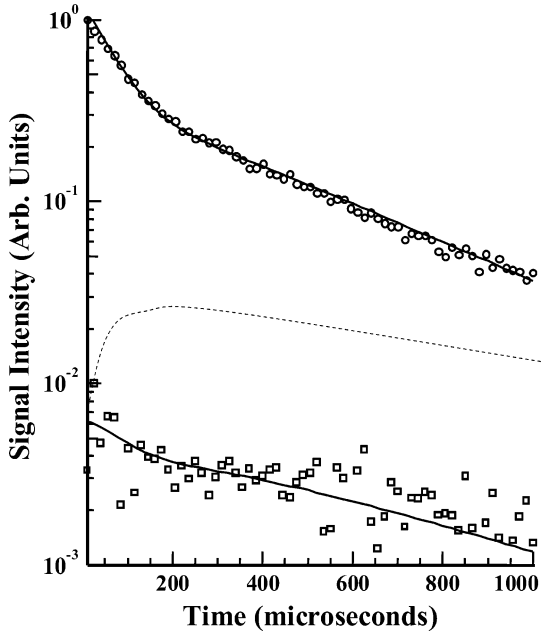


**Figure 13.** OH (□) and OD (○) decays measured from the OD + isoprene reaction in the presence of $O_2$ and NO. Solid lines represent simulations using the reaction mechanism and rate constants in Table 3. The dashed line represents the simulated OH concentration assuming direct hydrogen abstraction from the $\delta$-hydroxy alkoxy radicals by $O_2$ is comparable to the H-shift isomerization reaction of $\delta$-hydroxy alkoxy radicals. The concentrations of $[C_5H_8] = 7.5 \times 10^{13}$ molecules $cm^{-3}$, $[O_2] = 3.45 \times 10^{16}$ molecules $cm^{-3}$, and $[NO] = 10.4 \times 10^{14}$ molecules $cm^{-3}$.

photolysis and probe lasers powers between measurements and the OH at time zero is likely the result of residual $H_2O_2$ in the sample. Simulation of the two curves required modification of the oxidation mechanism to differentiate the sources of $HO_2$. The fit to the OH data was insensitive to the branching between alkoxy reaction channels. The best fit (solid line) to the OD data, however, required that the direct H-atom abstraction channel for the $\delta$-hydroxy alkoxy radicals was minor (10%). To fit the data, we have assumed an initial OH:OD ratio consistent with the signals at time zero. Also shown in the figure is the simulation (dotted line) resulting from a 50:50 branching between the direct H-atom abstraction channel and the isomerization channel. The simulation shows an initial rise due to the generation of OH from isoprene oxidation, a result that is not observed in our experiment.

## Conclusions

The present study is to understand isoprene oxidation mechanism by monitoring cyclic regeneration hydroxyl radical, and we have found that the branching ratio of the initial OH addition to the terminal carbon of isoprene molecule is preferred. The rate constant of $O_2$ addition reaction to the hydroxy alkyl radical is indirectly determined to be $(2.3 \pm 2.0) \times 10^{-12}$ molecule$^{-1}$ cm$^3$ s$^{-1}$ from the simulation of the reaction. The sensitivity analysis ensures that the experimental condition is suitable to determine the rate constant of the NO addition reaction to the hydroxy peroxy radicals and we have determined the rate constant of $(9.0 \pm 3.0) \times 10^{-12}$ molecule$^{-1}$ cm$^3$ s$^{-1}$. Very little generation of OH from the OD initiated isoprene oxidation implies H-shift isomerization is the major pathway for $\delta$-hydroxy alkoxy radicals.

**Supporting Information Available:** The detailed 44 reaction mechanism with rate constants and associated sensitivity analysis and fitting is available free of charge via the Internet at http://pubs.acs.org.

## References and Notes

(1) Chameides, W. L.; Fehsenfeld, F.; Rodgers, M. O.; Cardelino, C.; Martinez, J.; Parrish, D.; Lonneman, W.; Lawson, D. R.; Rasmussen, R. A.; Zimmerman, P.; Greenberg, J.; Middleton, P.; Wang, T. *J. Geophys. Res*. **1992**, *97*, 6037.

(2) Rasmussen, R. A.; Khalil, M. A. *J. Geophys. Res*. **1988**, *93*, 1417.

(3) Riemer, D. D.; Milne, P. J.; Farmer, C. T.; Zika, R. G. *Chemosphere* **1994**, *28*, 837.

(4) Starn, T. K.; Shepson, P. B.; Bertman, S. B.; Riemer, D. D.; Zika, R. G.; Olszyna, K. *Geophys. Res. Lett.* **1998**, *103*, 22437.

(5) Suh, I.; Lei, W.; Zhang, R. *J. Phys. Chem*. **2001**, *105*, 6471.

(6) Lei, W.; Zhang, R. *J. Phys. Chem. A* **2001**, *105*, 3808.

(7) McGivern, W. S.; Suh, I. S.; Clinkenbeard, A. D.; Zhang, R.; North, S. W. *J. Phys. Chem. A* **2000**, *104*, 6609.

(8) Stevens, P. S.; Seymour E.; Li, Z. *J. Phys. Chem. A* **2000**, *104*, 5989.

(9) Francisco-Márques, M.; Alvarez-Idaboy, J. R.; Galano, A.; Vivier-Bunge, A. *Phys. Chem. Chem. Phys.* **2003**, *5*, 1392

(10) Paulson S. E.; Seinfeld, J. H. *J. Geophys. Res.* **1992**, *97*, 20703.

(11) Tuazon, E. C.; Atkinson, R. *Int. J. Chem. Kinet.* **1989**, *21*, 1141.

(12) Jenkin, M. E.; Hayman, G. D. *J. Chem. Soc., Faraday Trans.* **1995**, *91*, 1911.

(13) Lei, W.; Zhang, R.; McGivern, W. S.; Derecskei-Kovacs, A.; North, S. W. *Chem. Phys. Lett.* **2000**, *326*, 109.

(14) Kleindienst, T. E.; Harris, G. W.; Pitts, J. N., Jr. *Environ. Sci. Technol*. **1982**, *16*, 844.

(15) Chuong, B.; Stevens, P. S. *J. Phys. Chem. A* **2000**, *104*, 5230.

(16) Iida, Y.; Obi, K.; Imamura, T. *Chem. Lett*. **2002**, *8*, 792.

(17) Atkinson, R.; Baulch, D. L.; Cox, R. A.; Crowley, J. N.; Hampson, R. F., Jr.; Kerr, J. A.; Rossi, M. J.; Troe, J. Summary of Evaluated Kinetic and Phtochemical Data for Atmospheric Chemistry. IUPAC Subcommittee on Gas Kinetic Data Evaluation for Atmospheric Chemistry; Blackwell: London, 2002.

(18) Campuzano-Jost, P.; Williams, M. B.; D'Ottone, L.; Hynes, A. *Geophys. Res. Lett.* **2000**, *27*, 693.

(19) Campuzano-Jost, P.; Williams, M. B.; D'Ottone, L.; Hynes, A. *J. Phys. Chem. A* **2003**, *109*, 1537.

(20) Park, J.; Jongsma, C. G.; Zhang, R.; North, S. W. *Phys. Chem. Chem. Phys.* **2003**, *5*, 3638.

(21) Lei, W.; Zhang, R.; McGivern, W. S.; Derecskei-Kovacs, A.; North, S. W. *J. Phys. Chem. A* **2001**, *105*, 471.
(22) Zhang, D.; Zhang, R.; Church, C.; North, S. W. *Chem. Phys. Lett. A* **2001**, *343*, 49.
(23) Zhang, R.; Suh, I.; Clinkenbeard, A.; Lei, W.; North, S. W. *J. Geophys. Res*. **2000**, *105*, 24627.
(24) Stevens, P.; L'Esperance, D.; Chuong, B.; Martin, G. *Int. J. Chem. Kinet.* **1999**, *31*, 637.
(25) Reitz, J. E.; McGivern, W. S.; Church, M. C.; Wilson, M. D.; North, S. W. *Int. J. Chem. Kinet.* **2002**, *34*, 255.
(26) Zhang, D.; Zhang, R.; North, S. W. *J. Phys. Chem. A* **2003**, *107*, 11013.
(27) Chuong, B.; Stevens, P. S. *J. Geophys. Res.* **2002**, *107*, 4162.
(28) Zhang, D.; Zhang, R.; Park, J.; North, S. W. *J. Am. Chem. Soc*. **2002**, *124*, 9600.
(29) Lohr, L. L.; Barker, J. R.; Shroll, R. M. *J. Phys. Chem. A* **2003**, *107*, 7429.
(30) Barker, J. R.; Lohr, L. L.; Shroll, R. M.; Reading, S. *J. Phys. Chem. A* **2003**, *107*, 7434.
(31) Sprengnether, M.; Demerjian, K. L.; Donahue, N. M.; Anderson, J. G. *J. Geophys. Res.* **2002**, *107*, 4268.
(32) Chen, X.; Hulbert, D.; Shepson, P. B. *J. Geophys. Res.* **1998**, *103*, 25563.
(33) DeMore, W. B.; Sander, S. P.; Golden, D. M.; Hampson, R. F.; Kurylo, M. J.; Howard, C. J.; Ravishankara, A. R.; Kolb, C. E.; Molina, M. J. Chemical Kinetics and Photochemical Data for Use in Stratospheric Modeling. JPL Publ. 02-25; Jet Propulsion Lab: Pasadena, CA, 2003.
(34) Eberhard, J.; Howard, C. J. *Int. J. Chem. Kinet.* **1996**, *28*, 731.
(35) Becker, K. H.; Geiger, H.; Wiesen, P. *Chem. Phys. Lett*. **1991**, *184*, 256.
(36) Park, J.; Stephens, J. C.; Zhang, R.; North, S. W. *J. Phys. Chem. A* **2003**, *107*, 6408.
(37) Dibble, T. S. *J. Phys. Chem. A* **2002**, *106*, 6643.
(38) It should be noted that the apparent low value of the alkoxy radical decomposition rate ($3.0 \times 10^4$ s$^{-1}$) reported in ref 25 is in fact consistent with the thermal decomposition rate at low pressures according to ref 36.
(39) Lloyd, A. C.; Atkinson, R.; Lurmann, F. W.; Nitta, B. *Atmos. Environ*. **1983**, *17*, 1931.
(40) Killus, J. P.; Whitten, G. Z. *Environ. Sci. Technol*. **1984**, *18*, 142.
(41) Arnts, R. R.; Gay, B. W., Jr. *Photochemistry of Some Naturally Emitted Hydrocarbons*; EPA-600/3-79-081; EPA: Washington, DC, 1979.
(42) Atkinson, R.; Aschmann, S. M.; Tuazon, E. C.; Arey, J.; Zielinska, B. *Int. J. Chem. Kinet.* **1989**, *21*, 593.
(43) Gu, C. I.; Rynard, C. M.; Hendry, D. G.; Mill, T. *Environ. Sci. Technol*. **1985**, *19*, 151.
(44) Tuazon, E. C.; Atkinson, R *Int. J. Chem. Kinet*. **1990**, *22*, 1221.
(45) Paulson, S. E.; Flagan, R. C.; Seinfeld, J. H. *Int. J. Chem. Kinet*. **1992**, *24*, 79.
(46) Grosjean, D.; Williams, E. L., II; Grosjean, E. *Environ. Sci. Technol*. **1993**, *27*, 830.
(47) Kwok, E. S.; Atkinson, R.; Arey, J. *Environ. Sci. Technol*. **1995**, *29*, 2467.
(48) Paulson, S. E.; Seinfeld, J. H. *J. Geophys. Res.* **1992**, *97*, 20703.
(49) Tuazon, E. C.; Atkinson, R. *Int. J. Chem. Kinet.* **1990**, *22*, 1221.
(50) Atkinson, R.; Aschmann, S. M.; Tuazon, E. C.; Arey, J.; Zielinska, B. *Int. J. Chem. Kinet.* **1989**, *27*, 593.
(51) Miyoshi, A.; Hatakeyama, S.; Washida, N. *J. Geophys. Res.* **1994**, *99*, 18779.
(52) Atkinson, R.; Baulch, D. L.; Cox, R. A.; Hampson, R. F., Jr.; Kerr, J. A.; Rossi, M. J.; Troe, J. *J. Phys. Chem. Ref. Data* **1997**, *26*, 1329.
(53) Troe, J. *J. Chem. Phys.* **1977**, *66*, 4745.
(54) DeMore, W. B.; Sander, S. P.; Golden, D. M.; Hampson, R. F.; Kurylo, M. J.; Howard, C. J.; Ravishankara, A. R.; Kolb, C. E.; Molina, M. J. *Chemical kinetics and photochemical data for use in stratospheric modeling*"; JPL Publ. 92, NASA Jet Propulsion Laboratory: Pasadena, CA, 1992.
(55) For example, the low-pressure termolecular rate constant for $CH_3 + O_2$ shows a similar difference between He and Ar buffer gas. Selzer E. A.; Bayes, K. D. *J. Phys. Chem*. **1983**, *87*, 392.
(56) Ianni, J. C. Kintecus, Windows Version 2.80, 2002, www.kintecus.com.
(57) The sensitivity analysis and representative fits associated with the 44 step mechanism is also provided in the Supporting Information.
(58) Corresponding to 93% OH addition to the terminal carbons and 7% addition to the internal carbons.
(59) Peeters, J.; Boullart, W.; Hoeymissen, J. V. In *Proceedings of EUROTRAC Symposium '94*; Borrell, P. M., et al., Eds.; SPB Academic Publishing: The Hague, The Netherlands, 1994; p 110.
(60) Atkinson, R. *J. Phys. Chem. Ref. Data* **1997**, *26*, 215.
(61) Lotz, Ch.; Zellner, R. Phys. *Chem. Chem. Phys*. **2001**, *3*, 2607.
(62) Deng, W.; Wang, C.; Katz, D. R.; Gawinski, G. R.; Davis, A. J.; Dibble, T. S. *Chem. Phys. Lett*. **2000**, *330*, 541.
(63) Blitz, M.; Pilling, M. J.; Robertson, S. H.; Seakins, P. W. *Phys. Chem. Chem. Phys*. **1999**, *1*, 73.
(64) Steinfeld, J. I.; Francisco, J. S.; Hase, W. L. *Chemical Kinetics and Dynamics*; Prentice Hall International, Inc.: Englewood Cliffs, NJ, 1989.
(65) Schested, J.; Nielson, O. J.; Wallington, T. J. *Chem. Phys. Lett*. **1993**, *213*, 457.
(66) Miyoshi, A.; Hiroyuki, M.; Washida, N. *J. Phys. Chem*. **1990**, *94*, 3016.
(67) Koch, R.; Siese, M.; Fittschen, C.; Zetzsch, C. In a contribution to the EUROTRAC subproject LACTOZ, 1995; p 268.
(68) At low $O_2$ concentrations the $R + O_2$ rate constant ($k_3$) is sensitive to the NO termination rate. Varying this rate from $3 \times 10^{-11}$ to $1 \times 10^{-10}$ molecule$^{-1}$ cm$^3$ s$^{-1}$ results in the rather large error bars associated with $k_2$. We do not anticipate the termination reaction to exceed these limits on the basis of studies of analogous systems.
(69) Zhao, J.; Zhang. R.; North, S. W. *Chem. Phys. Lett.* **2003**, *369*, 204.
(70) Jenkin, M. E.; Boyd, A. A.; Lesclaux, R. *J. Atmos. Chem.* **1998**, *29*, 267.
(71) Zhao, J.; Zhang, R.; Fortner, E. C.; North, S. W. *J. Am. Chem. Soc.* **2004**, *126*, 2686.